Acta Crystallographica Section D
Biological Crystallography
ISSN 0907-4449

Structural insights into the role of the Chl4–Iml3 complex in kinetochore assembly

Qiong Guo,[a,b] Yuyong Tao,[a,b] Hejun Liu,[a,b] Maikun Teng[a,b]* and Xu Li[a,b]*

[a]Hefei National Laboratory for Physical Sciences at Microscale and School of Life Sciences, University of Science and Technology of China, Hefei, Anhui 230026, People's Republic of China, and [b]Key Laboratory of Structural Biology, Chinese Academy of Sciences, Hefei, Anhui 230026, People's Republic of China

Correspondence e-mail: mkteng@ustc.edu.cn, sachem@ustc.edu.cn

Received 16 May 2013
Accepted 9 August 2013

PDB Reference: Iml3, 4kr1

Human CENP-N and CENP-L have been reported to selectively recognize the CENP-A nucleosome and to contribute to recruiting other constitutive centromere-associated network (CCAN) complexes involved in assembly of the inner kinetochore. As their homologues, Chl4 and Iml3 from budding yeast function in a similar way in *de novo* assembly of the kinetochore. A lack of biochemical and structural information precludes further understanding of their exact role at the molecular level. Here, the crystal structure of Iml3 is presented and the structure shows that Iml3 adopts an elongated conformation with a series of intramolecular interactions. Pull-down assays revealed that the C-terminal domain of Chl4, which forms a dimer in solution, is responsible for Iml3 binding. Acting as a heterodimer, the Chl4–Iml3 complex exhibits a low-affinity nonspecific DNA-binding activity which may play an important role in the kinetochore-assembly process.

1. Introduction

Faithful transmission of the eukaryotic genome in mitosis and meiosis is essential for successful cell division. This process depends on the kinetochore, which is a large multi-protein complex that assembles at the centromeric DNA of chromosomes and provides attachment sites for the microtubule plus ends (De Wulf *et al.*, 2003; Fitzgerald-Hayes *et al.*, 1982). This connection is indispensable for precise chromosome segregation and thus ensures genetic stability (Westermann & Schleiffer, 2013); defects in this stability can result in aneuploidy and lead to congenital disorders, cancers and cell death (Yuen *et al.*, 2005). Despite a marked divergence of centromeric DNA sequences among vertebrates (Okada *et al.*, 2006), the centromeric DNA in budding yeast exhibits typical signatures and can be subdivided into CDEI, CDEII and CDEIII regions (Santaguida & Musacchio, 2009). CDE I (8 bp) and CDE III (25 bp) are highly conserved, whereas CDE II lies between CDE I and CDE III and contains a degenerate A/T-rich sequence (Cleveland *et al.*, 2003).

In contrast, the kinetochore structure and composition is highly conserved from yeast to humans (Okada *et al.*, 2006; Musacchio & Salmon, 2007; Cheeseman *et al.*, 2008; Welburn & Cheeseman, 2008). A network of proteins comprise the fully functional kinetochore, which exhibits a two-layer structure, namely the inner and the outer kinetochore (Hori *et al.*, 2008). The outer kinetochore contributes to linking the kinetochore to the microtubules through Knl-1–Mis12–Ndc80 network complexes (Spc105, MIND and Ndc80, respectively, in budding yeast; Carroll *et al.*, 2009; Santaguida & Musacchio,

2009). The inner layer is closely opposed to centromeric DNA and is responsible for kinetochore assembly on the chromosomes (Okada *et al.*, 2006). The inner kinetochore contains specialized nucleosomes in which histone H3 is replaced by the histone H3 variant CENP-A, which is an epigenetic marker that specifies the identity of the centromere (Carroll *et al.*, 2009; Foltz *et al.*, 2006). In mammals, the protein network denoted the constitutive centromere-associated network (CCAN) complex has been reported to construct the inner kinetochore (Takeuchi & Fukagawa, 2012; Hori *et al.*, 2013; McAinsh & Meraldi, 2011). Of these proteins, the CENP-N protein has been shown to selectively recognize the CENP-A nucleosomes in a DNA sequence-independent manner during the first step of kinetochore assembly and then facilitates the subsequent recruitment of other CCAN elements at the centromere through its direct interaction with CENP-L (Santaguida & Musacchio, 2009; Carroll *et al.*, 2009; Eskat *et al.*, 2012). Most CCAN proteins have homologues in budding yeast, which implies that the mechanism underlying kinetochore assembly has occurred similarly during evolution. For example, as the homologue of CENP-N, the Chl4 protein from budding yeast exhibits similar functions to CENP-N: the *de novo* assembly of centromeres (Mythreye & Bloom, 2003; Westermann & Schleiffer, 2013). As revealed by yeast-hybrid and co-immunoprecipitation analyses, Chl4 binds to Iml3, which is proposed to be the homologue of CENP-L in mammals (Westermann & Schleiffer, 2013). This subcomplex belongs to the Ctf19 complex (Lahiri *et al.*, 2013), which contains several other CCAN homologues (Hyland *et al.*, 1999; Ortiz *et al.*, 1999). A recent study showed that Iml3 is distinct from Chl4 at the kinetochore. Iml3 may act as a link between the inner and the outer complexes and thus contributes to the construction of a complete kinetochore (Lahiri *et al.*, 2013). Nevertheless, the Iml3 protein may function similarly to CENP-L and may mediate interactions between the different complexes involved in kinetochore assembly.

Despite the defined functional importance of CENP-N–CENP-L in initial kinetochore assembly, the structures that interact with each other and with the DNA-containing CENP-A nucleosome remain unknown. In this manuscript, we report the crystal structure of Iml3 from *Saccharomyces cerevisiae* and further characterize its interaction with Chl4. We also demonstrate that the Chl4–Iml3 complex possesses non-specific DNA-binding activity, which may be of great value for the recognition of the CENP-A nucleosome in mammals. The structural and biochemical results from this study provide further insight for understanding the kinetochore-assembly process.

2. Materials and methods

2.1. Protein expression and purification

Iml3 and different truncations of Chl4 were cloned into a modified pET28a vector with a His-MBP tag followed by a TEV cleavage site at the N-terminus of the recombinant protein. After overexpression in *Escherichia coli* Rosetta (DE3)

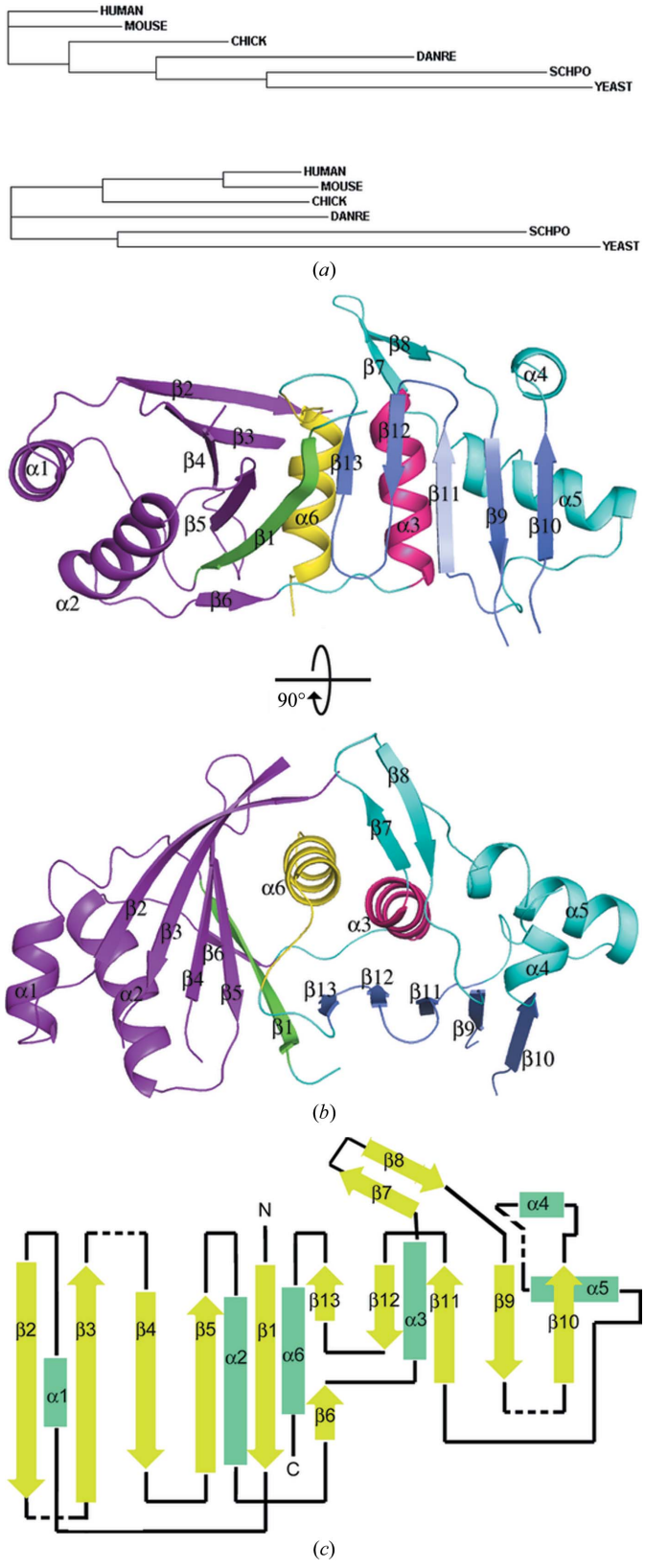

Figure 1
Overall structure of Iml3 and the phylogenetic tree of CENP-N and CENP-L. (*a*) A phylogenetic tree showing the relationships of CENP-N homologues (top) and CENP-L homologues (bottom) from different species in eukaryotes. (*b*) Ribbon representation of Iml3. The top view is an orthogonal view from the top of the bottom view. (*c*) Topological structure of Iml3. Invisible residues are shown as black dashed lines.

cells, the proteins were subjected or were not subjected to TEV digestion at 277 K overnight and were further purified using HiTrap Q FF (5 ml) and HiLoad 16/60 Superdex 200 (GE Healthcare). The proteins were then concentrated to 30–40 mg ml^{-1} in 20 m*M* Tris–HCl pH 7.5, 50 m*M* NaCl, 1 m*M* DTT. SeMet-derivative Iml3 was prepared using *E. coli* strain B834 (Novagen) and was then purified by a procedure similar to that described above.

2.2. Crystallization and structure determination

Crystals of SeMet-derivative Iml3 were grown using the hanging-drop vapour-diffusion method at 285 K. The crystals appeared using a buffer consisting of 3 *M* sodium formate pH 7.0, 100 m*M* CsCl, 2–5% PEG 4000. SAD data were collected on beamline BL17U of the Shanghai Synchrotron Radiation Facility (SSRF) and were processed using *HKL*-2000 (Otwinowski & Minor, 1997) and programs from the *CCP*4 package (Winn *et al.*, 2011). The phases were calculated using the *AutoSol* GUI in *PHENIX* (Adams *et al.*, 2010) and the initial model was built using the *AutoBuild* program in *PHENIX* (Adams *et al.*, 2010). Further refinement was carried out using *Coot* (Emsley & Cowtan, 2004), *REFMAC*5 (Murshudov *et al.*, 2011) and *phenix.refine* (Adams *et al.*, 2010). The structure was checked in its entirety using *MolProbity* (Chen *et al.*, 2010) and the figures were prepared using *PyMOL* (Schrödinger).

2.3. Size-exclusion chromatography assays

Size-exclusion chromatography assays were performed on a Superdex 200 column (10/300 GL; GE Healthcare). The protein sample or molecular-mass standards were applied to the column and were eluted with 50 m*M* Tris–HCl pH 7.5, 200 m*M* NaCl, 1 m*M* DTT. The standard proteins (GE Healthcare) were β-amylase (200.0 kDa), alcohol dehydrogenase (150.0 kDa), albumin (66.0 kDa), carbonic anhydrase (29.0 kDa) and cytochrome *c* (12.4 kDa). The void volume was determined with blue dextran (GE Healthcare).

2.4. Pull-down assays

A similar amount of purified Iml3 was added to a similar amount of *E. coli* cells expressing recombinant His-MBP-Chl4 or His-MBP-Iml3 fragments. The mixture was lysed and the supernatant was incubated with 100 µl Ni–NTA beads for 30 min at room temperature. The beads were washed two times with binding buffer supplemented with 50 m*M* imidazole. The bound proteins eluted from the beads were resolved by SDS–PAGE (12%) and stained with Coomassie Brilliant Blue.

2.5. Electrophoretic mobility-shift assay (EMSA)

DNA-binding reactions (10 µl) were conducted for 1 h at 277 K in binding buffer (20 m*M* Tris–HCl pH 7.5, 50 m*M* NaCl, 1 m*M* DTT) with the indicated protein concentration and 0.6 µ*M* DNA substrate. After the addition of 3 µl gel-loading buffer (50% glycerol, 0.02% bromophenol blue), the reaction mixtures were resolved on a 5% native polyacrylamide gel in 0.5× TBE buffer at 277 K for 60 min and visualized by Gel-Red staining. The double-stranded DNA (dsDNA) substrates were formed by annealing single-stranded *CEN3* DNA (TATTAGTGTATTTGATTTCCGAAAGTT) with its complementary DNA. The dsDNA-1, AT-rich and GC-only sequences were ACGCTGCCGAATTCTACCAGTGCCTTGCTAGGACATCTTTGCCCACCTGCAGGTTCACC, GGCATTAAATAATATTAATTATAATCC and CCCGGCGGGCGGCCCGGCGGCCCGGCC, respectively.

Table 1
Data-collection and refinement statistics for SeMet-derivative Iml3.

Values in parentheses are for the highest resolution shell.

Data collection	
Space group	$P6_322$
Unit-cell parameters (Å, °)	$a = b = 73.0$, $c = 188.8$, $\alpha = \beta = 90.00$, $\gamma = 120.00$
Wavelength (Å)	0.9795
Resolution (Å)	50.00–2.50 (2.54–2.50)
Unique reflections	11039 (528)
Multiplicity	20.2 (20.6)
$R_{\rm merge}$† (%)	10.1 (68.6)
$\langle I/\sigma(I)\rangle$	35.9 (5.5)
Completeness (%)	99.9 (100)
Refinement	
Resolution	47.21–2.50 (2.56–2.50)
Unique reflections	10430 (725)
$R_{\rm work}$‡ (%)	23.7 (32.1)
$R_{\rm free}$‡ (%)	26.2 (30.9)
Stereochemistry, residues in	
Favoured region (%)	97.1
Allowed region (%)	2.9
No. of residues	219
No. of protein atoms	1675
B factors (Å^2)	
Protein main chain	49.1
Protein side chain	43.5
R.m.s.d.	
Bond lengths (Å)	0.007
Bond angles (°)	0.988

† $R_{\rm merge} = \sum_{hkl}\sum_i |I_i(hkl) - \langle I(hkl)\rangle| / \sum_{hkl}\sum_i I_i(hkl)$, where $I_i(hkl)$ is the intensity of an individual reflection and $\langle I(hkl)\rangle$ is the average intensity of that reflection. ‡ $R_{\rm work} = \sum_{hkl} ||F_{\rm obs}| - |F_{\rm calc}|| / \sum_{hkl} |F_{\rm obs}|$ for all reflections and $R_{\rm free} = \sum_{hkl} ||F_{\rm obs}| - |F_{\rm calc}|| / \sum_{hkl} |F_{\rm obs}|$ calculated on the 5% of data excluded from refinement.

3. Results and discussion

3.1. Structure determination and overall structure

Most of the CCAN proteins described to date do not contain easily identified domains, the exceptions being those with a histone fold or DNA-binding motifs (Westermann & Schleiffer, 2013). The same is true for CENP-N and CENP-L and their homologues (Fig. 1*a*). Thus, resolving the structures of these proteins would further advance our understanding of the kinetochore. Although we successfully obtained a stable Chl4–Iml3 complex (see below), we failed to acquire a crystal after numerous attempts. Although a native data set was collected for Iml3, the lack of a homologous model for molecular replacement prompted us to prepare selenomethionine-labelled crystals. A complete single-wavelength anomalous dispersion (SAD) data set indexed in space group $P6_322$ was collected from a single selenomethionine derivative. The SAD data were then used to calculate the phases.

The final model, which was refined at a resolution of 2.5 Å, contains 219 residues and all of the residues exhibit acceptable geometry as determined by *MolProbity* (Chen *et al.*, 2010). The data-collection and refinement statistics are presented in Table 1. The determined structure shows that Iml3 contains six α-helices and 13 β-strands (Figs. 1*b* and 1*c*). Notably, all of the β-strands are packed in an antiparallel manner; 11 of them are continuous and form an extended β-sheet, yielding an elongated Iml3 conformation. The α-helices of Iml3 flank both sides of the β-sheet to support the formation of a compact structure (Fig. 1*b*).

3.2. Protein fold

An unbiased search of the Protein Data Bank using *DALI* failed to detect any structures bearing an overall resemblance to that of Iml3. Therefore, the Iml3 structure represents a novel fold, which is consistent with the uniqueness of the primary sequence. The most prominent feature of the Iml3 structure is the heavily arched β-sheet composed of 11 β-strands that forms an incomplete barrel at one end and a twisted plane at the other end (Fig. 2*a*). The β1 strand stands out because it mediates the formation of this type of two-β-sheet structure. On one hand, it bends markedly at its N-terminal end to interact with the β13 strand in the twisted plane; on the other hand, its C-terminus packs against the β6 strand from the incomplete barrel (Fig. 2*b*). The element immediately after the C-terminus is the α3 helix, which contributes to the stabilization of the intact structure. Immediately after the α3 helix, the β7 and β8 strands protrude from the structural core (Fig. 2*b*). Similarly to two arms, the protruding strands may be involved in recognition of and regulation by the Iml3-binding partners.

Rather than acting as two separate domains, the incomplete barrel and twisted plane are bridged in one structural unit by two connecting helices, namely the α3 and the α6 helices (Fig. 2*a*). The convex surface of the barrel is flanked by the α1 and α2 helices and its concave side is filled by the α6 helix, which shields the hydrophobic surface from the solvent (Fig. 2*c*). Meanwhile, the α6 helix makes loose contacts with the α3 helix in an antiparallel manner and the α3 helix in turn is packed on the outer face of the twisted plane (Fig. 2*d*). Thus, a series of intramolecular interactions ensure that Iml3 adopts a compact structure that resembles a single folded unit.

3.3. Chl4–Iml3 interaction

Previous studies have revealed that Iml3 and Chl4 interact with each other and form a stable complex *in vivo* (Pot *et al.*, 2003). To better characterize this interaction, we conducted pull-down assays to determine the Iml3-interaction domain within Chl4. A series of Chl4 deletion mutants were constructed using the MBP-fusion form (Fig. 3*a*). As shown in Figs. 3(*a*) and 3(*b*), the Chl4 C-terminal region consisting of residues 378–458 is sufficient for Iml3 binding. We were unable to test the binding affinity of Iml3 towards full-length Chl4 (FL-Chl4) owing to the lack of expression of FL-Chl4 in *E. coli*. However, because the longer fragment consisting of residues 261–458 exhibits an Iml3-binding affinity that is indistinguishable from that of the shorter fragment (residues 378–458; Fig. 3*b*), we conclude that the C-terminus of Chl4 is responsible for Iml3 binding, which is consistent with the

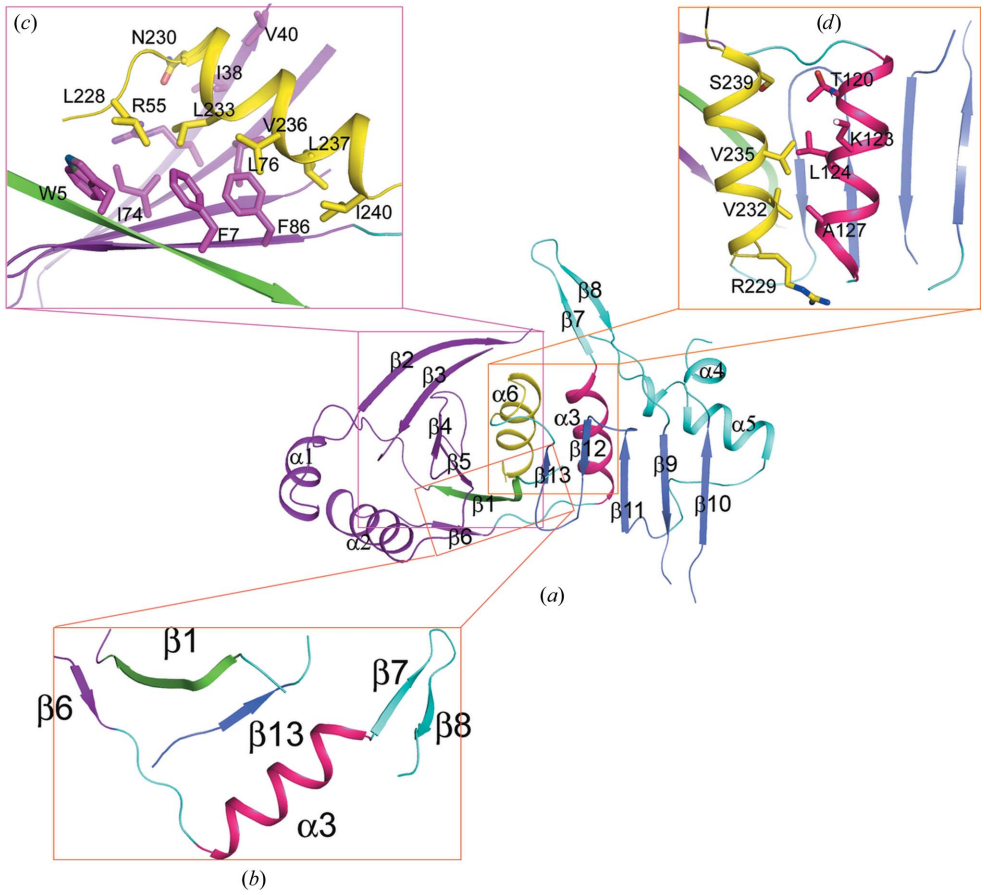

Figure 2
Structural features of Iml3. (*a*) The β-barrel and twisted plane. The β-strands forming the barrel are shown in purple, except for β1, which is highlighted in green. The twisted plane is shown in blue. (*b*) The interaction mode among the β1, β6 and β13 strands. The α3 helix (pink) is followed by the β7 and β8 strands (cyan). (*c*) The hydrophobic interactions between α6 (yellow) and the β-barrel. Residues involved in the interactions are labelled and shown as sticks. (*d*) The loose interactions between the α3 (pink) and α6 helices. Residues making contacts are shown as sticks. The α3 helix packs against the twisted plane.

binding pattern of the homologous proteins CENP-N and CENP-L (Eskat *et al.*, 2012).

Based on the above results, we constructed two further shorter fragments consisting of Chl4 residues 378–426 and 420–458 to determine the dominant region. As shown in Fig. 3(*c*), both fragments, particularly Chl4$^{420–458}$, exhibited reduced binding affinity toward Iml3 with respect to Chl4$^{378–458}$, which indicates that both regions are essential for efficient Iml3 binding. According to secondary-structure prediction, Chl4$^{378–458}$ may be flexible because both of its ends are random coils; thus Chl4$^{378–458}$ may wrap itself around Iml3 during interaction. After a detailed inspection of the Iml3 structure, we found that there were several missing residues between the α4 and the α5 helices (Fig. 1*b*). In addition, these two helices exhibited a higher *B* factor relative to the other regions (Fig. 3*d*). We speculated that this area may thus be the Chl4-binding area and that it becomes flexible in the absence of its binding partner Chl4 (Fig. 3*d*).

3.4. Solution behaviour

Although there is only one Iml3 molecule in the asymmetric unit, the protein forms a symmetrical dimer through the antiparallel interaction of the β10 and β10′ strands from two neighbouring Iml3 molecules in the crystal lattice (Fig. 4*a*). Six hydrogen bonds are formed between the two segments consisting of the β10 strand and the flanking α4 helix (Fig. 4*a*). A total buried surface of 516 Å^2 suggests that Iml3 may exist as a dimer in solution. Iml3 elutes with a molecular weight of approximately 43 kDa on size-exclusion chromatography, and this size is larger than the theoretical value of 28 kDa for the Iml3 monomer, but lower than the molecular weight of a dimer (Fig. 4*b*). Thus, considering the elongated rather than globular shape of Iml3, which may induce a smaller retention volume, Iml3 is most likely to be a monomer in solution, as was confirmed by the gel-filtration result obtained for MBP-fusion Iml3 (Fig. 4*b*). To gain further evidence, pull-down assays using MBP-Iml3 and Iml3 alone were employed and a similar result was obtained (Fig. 4*c*).

In contrast to the monomerization of Iml3, Chl4$^{378–458}$ appears to migrate as a dimer in solution, as revealed by both Chl4$^{378–458}$ alone and the MBP-fusion form (Fig. 4*d*). Interestingly, when Chl4$^{378–458}$ was complexed with Iml3 its intermolecular association was eliminated and it formed a heterodimer with Iml3 based on the elution volume (Fig. 4*d*). In other words, Iml3 may bind to a Chl4 surface that could mediate Chl4 self-association in the absence of Iml3. How these interactions occur and their associated significance require further study of the structure of the complex. In summary, Iml3 may function as a heterodimer with Chl4 during assembly of the inner kinetochore and CENP-N may also exhibit the same function with CENP-L.

3.5. Structural implications

Although Iml3 has a unique fold, the β-sheet twisted plane shows similarity to *E. coli* RdgC and *Arabidopsis thaliana* TBP (Figs. 5*a*, 5*b* and 5*c*). Both RdgC and TBP possess a broad solvent-accessible β-sheet surface (Figs. 5*a* and 5*c*). Of particular note is that both of these proteins interact with DNA through positively charged residues located on the inner surface of the β-sheet (Briggs *et al.*, 2007; Patikoglou *et al.*, 1999). Interestingly, the calculated electrostatic surface potential of Iml3 also exhibits a positive charge on the inner face, which is most likely to be involved in DNA binding (Fig. 5*d*). Moreover, some of the basic residues in the β-sheet are conserved among fungal orthologues (Fig. 5*e*), which

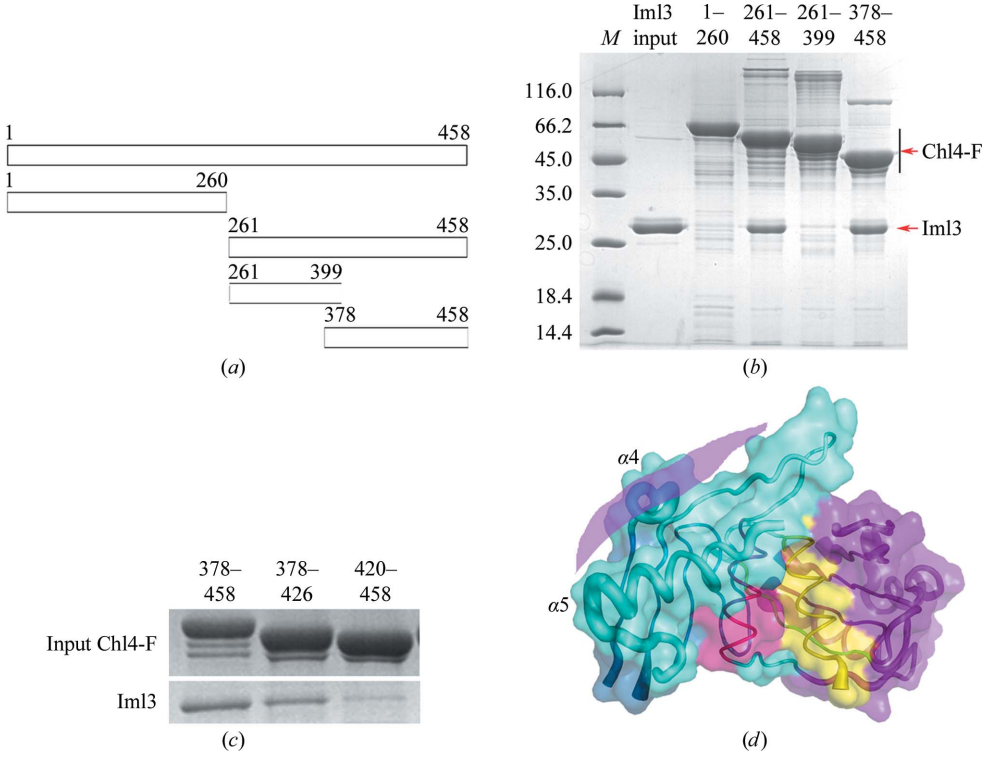

Figure 3
The interaction between Chl4 and Iml3. (*a*) Experimental scheme used to map the Iml3-interaction domain within Chl4. (*b*) Pull-down assays. The His-MBP-Chl4 fragment (Chl4-F) was used to pull down purified Iml3. The region consisting of residues 378–458 is sufficient for Iml3 binding. Lane *M* contains molecular-mass markers (labelled in kDa). (*c*) Detailed interaction tests between Iml3 and Chl4. Both fragments, the N-terminal fragment (Chl4$^{378–426}$) and its C-terminal counterpart (Chl4$^{420–458}$), are essential for efficient Iml3 binding. (*d*) *B*-factor distribution of Iml3. The wider the tubing, the higher the *B* factor. The Chl4 may bind the region of Iml3 indicated by the purple shadow.

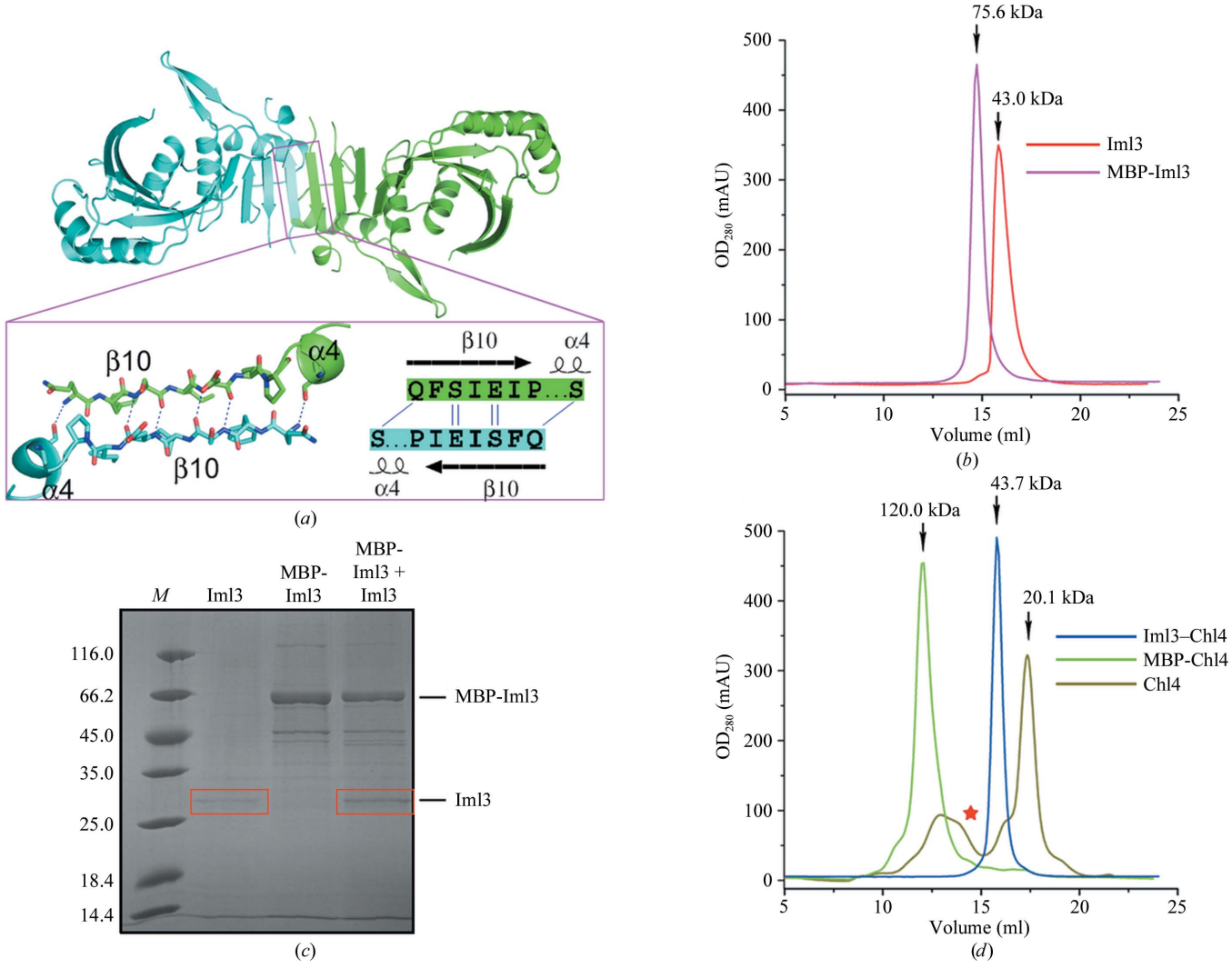

Figure 4
Iml3 forms a heterodimer with Chl4. (*a*) The Iml3 dimer in the crystal packing. The bottom close-up view indicates the residues and hydrogen bonds present in the dimer interface. (*b*) Gel-filtration analysis of Iml3. Iml3 and MBP-Iml3 (theoretical molecular weight 71.2 kDa) elute with molecular weights of about 43.0 and 75.6 kDa, respectively. Lane *M* contains molecular-mass markers (labelled in kDa). (*c*) Pull-down assays between MBP-Iml3 and Iml3. The red boxes indicate the position of Iml3. The Iml3 eluted together with MBP-Iml3 may be caused by nonspecific binding compared with Iml3 alone. (*d*) Gel-filtration analysis of the Iml3–Chl4 complex. The peak indicated by a red star is caused by contaminant proteins. The theoretical molecular weights of individual Chl4$^{378–458}$ and MBP-Chl4$^{378–458}$ and the Iml3–Chl4$^{378–458}$ dimer are 8.9, 52.0 and 36.8 kDa, respectively.

suggests that DNA binding is a common feature of these proteins. Choosing *CEN3* dsDNA and random-sequence dsDNA as the substrate, we employed EMSA to query whether the Chl4–Iml3 complex can bind to DNA. Neither Iml3 nor Chl4 alone binds to DNA (Fig. 5*f*); however, the Chl4–Iml3 complex shows low binding affinity towards all types of DNA and thus displays nonspecific DNA-binding activity (Fig. 5*g* and Supplementary Fig. S1[1]). Thus, Iml3 may cooperate with Chl4 in DNA binding, which is a common phenomenon, as described in our previous study (Tao, Jin *et al.*, 2012; Tao, Li *et al.*, 2012). The nonspecific DNA-binding activity of the Chl4–Iml3 complex may play an important role in *de novo* assembly of the inner kinetochore and this activity may also be exhibited by the CENP-N–CENP-L complex. As shown previously, CENP-N can recognize the CENP-A nucleosome but not the CENP-A–H4 tetramer (Carroll *et al.*, 2009). Whether CENP-N alone can directly bind to DNA remains to be addressed. It appears that the DNA in the nucleosome, in addition to the protein element, is another anchor site for CENP-N–CENP-L (Carroll *et al.*, 2009). The interaction between CENP-N and the CENP-A nucleosome can occur only after both of these requirements are satisfied. Complexation with CENP-L may further strengthen the association of CENP-N with the nucleosome and the assembly process can then be initiated properly and efficiently.

In summary, our structural and biochemical analyses of the Chl4–Iml3 complex have provided new insights into the novel fold-mediated molecular state of Iml3 and have advanced our

[1] Supplementary material has been deposited in the IUCr electronic archive (Reference: CB5037). Services for accessing this material are described at the back of the journal.

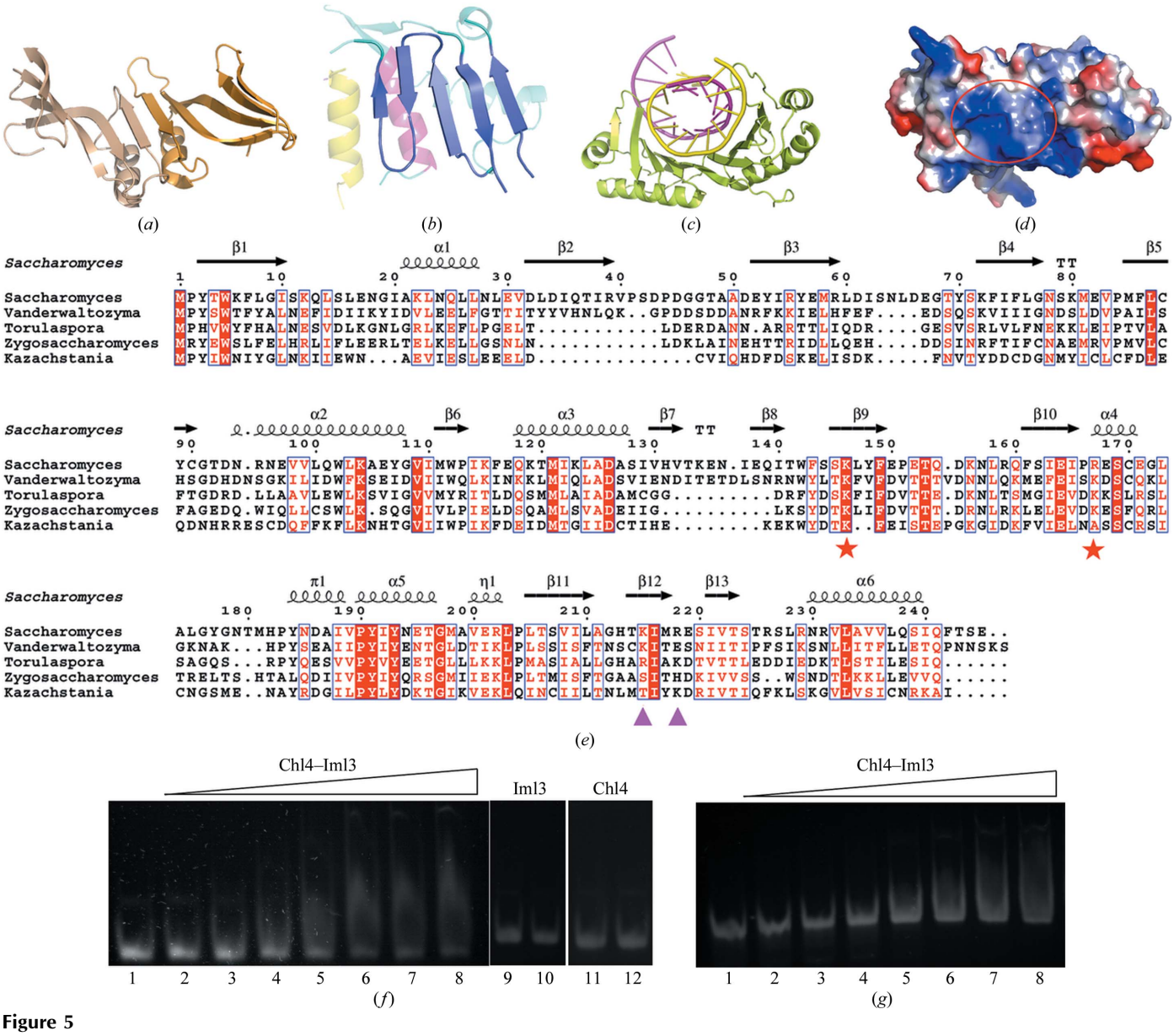

Figure 5
The Chl4–Iml3 complex binds to DNA. (*a*) The helical surface of RdgC (PDB entry 2owl; Briggs *et al.*, 2007). The inner face of the RdgC hole is rich in positively charged residues involved in DNA binding. (*b*) The twisted plane of Iml3. It shares structural similarity with RdgC and TBP. (*c*) The TBP–DNA structure (PDB entry 1qnc; Patikoglou *et al.*, 1999). The inner face of the β-sheet is where DNA binds. (*d*) Calculated electrostatic surface of Iml3. The twisted plane is circled by a red line. (*e*) Sequence alignment among the fungal Iml3 orthologues. The basic residues in the β-sheet which may interact with DNA are highly conserved (indicated by a red star) or less conserved (indicated by a pink triangle). (*f*) EMSA results of the Chl4–Iml3 complex with *CEN3* DNA. 0.6 µ*M* *CEN3* dsDNA substrate with the following proteins: lanes 1–8, 0, 0.5, 1, 2, 4, 6, 8 and 10 µ*M* Chl4–Iml3, respectively; lanes 9 and 10, 0 and 10 µ*M* Iml3, respectively; lanes 11 and 12, 0 and 10 µ*M* Chl4$^{378–458}$, respectively. As the protein concentration increases, less free-form DNA is observed. (*g*) EMSA results of the Chl4–Iml3 complex with random dsDNA 1. 0.6 µ*M* random dsDNA with 0, 0.5, 1, 2, 4, 6, 8 and 10 µ*M* protein in lanes 1–8, respectively.

understanding of the interaction between Chl4 and Iml3. The results of this study should facilitate further in-depth analyses of the molecular mechanism of kinetochore assembly.

We are grateful to the staff members at SSRF for the collection of diffraction data. Financial support for this project was provided by the Chinese Ministry of Science and Technology (grant Nos. 2009CB825500 and 2012CB917200), the Chinese National Natural Science Foundation (grant Nos. 31130018, 30900224 and 10979039) and the Science and Technological Fund of Anhui Province for Outstanding Youth (grant No. 10040606Y11).

References

Adams, P. D. *et al.* (2010). *Acta Cryst.* D**66**, 213–221.
Briggs, G. S., McEwan, P. A., Yu, J., Moore, T., Emsley, J. & Lloyd, R. G. (2007). *J. Biol. Chem.* **282**, 12353–12357.
Carroll, C. W., Silva, M. C., Godek, K. M., Jansen, L. E. & Straight, A. F. (2009). *Nature Cell Biol.* **11**, 896–902.
Cheeseman, I. M., Hori, T., Fukagawa, T. & Desai, A. (2008). *Mol. Biol. Cell*, **19**, 587–594.

Chen, V. B., Arendall, W. B., Headd, J. J., Keedy, D. A., Immormino, R. M., Kapral, G. J., Murray, L. W., Richardson, J. S. & Richardson, D. C. (2010). *Acta Cryst.* D**66**, 12–21.
Cleveland, D. W., Mao, Y. & Sullivan, K. F. (2003). *Cell*, **112**, 407–421.
De Wulf, P., McAinsh, A. D. & Sorger, P. K. (2003). *Genes Dev.* **17**, 2902–2921.
Emsley, P. & Cowtan, K. (2004). *Acta Cryst.* D**60**, 2126–2132.
Eskat, A., Deng, W., Hofmeister, A., Rudolphi, S., Emmerth, S., Hellwig, D., Ulbricht, T., Döring, V., Bancroft, J. M., McAinsh, A. D., Cardoso, M. C., Meraldi, P., Hoischen, C., Leonhardt, H. & Diekmann, S. (2012). *PLoS One*, **7**, e44717.
Fitzgerald-Hayes, M., Clarke, L. & Carbon, J. (1982). *Cell*, **29**, 235–244.
Foltz, D. R., Jansen, L. E., Black, B. E., Bailey, A. O., Yates, J. R. III & Cleveland, D. W. (2006). *Nature Cell Biol.* **8**, 458–469.
Hori, T., Amano, M., Suzuki, A., Backer, C. B., Welburn, J. P., Dong, Y., McEwen, B. F., Shang, W.-H., Suzuki, E., Okawa, K., Cheeseman, I. M. & Fukagawa, T. (2008). *Cell*, **135**, 1039–1052.
Hori, T., Shang, W.-H., Takeuchi, K. & Fukagawa, T. (2013). *J. Cell Biol.* **200**, 45–60.
Hyland, K. M., Kingsbury, J., Koshland, D. & Hieter, P. (1999). *J. Cell Biol.* **145**, 15–28.
Lahiri, S., Mehta, G. D. & Ghosh, S. K. (2013). *FEMS Yeast Res.* **13**, 375–385.
McAinsh, A. D. & Meraldi, P. (2011). *Semin. Cell Dev. Biol.* **22**, 946–952.
Murshudov, G. N., Skubák, P., Lebedev, A. A., Pannu, N. S., Steiner, R. A., Nicholls, R. A., Winn, M. D., Long, F. & Vagin, A. A. (2011). *Acta Cryst.* D**67**, 355–367.
Musacchio, A. & Salmon, E. D. (2007). *Nature Rev. Mol. Cell Biol.* **8**, 379–393.
Mythreye, K. & Bloom, K. S. (2003). *J. Cell Biol.* **160**, 833–843.
Okada, M., Cheeseman, I. M., Hori, T., Okawa, K., McLeod, I. X., Yates, J. R. III, Desai, A. & Fukagawa, T. (2006). *Nature Cell Biol.* **8**, 446–457.
Ortiz, J., Stemmann, O., Rank, S. & Lechner, J. (1999). *Genes Dev.* **13**, 1140–1155.
Otwinowski, Z. & Minor, W. (1997). *Methods Enzymol.* **276**, 307–326.
Patikoglou, G. A., Kim, J. L., Sun, L., Yang, S.-H., Kodadek, T. & Burley, S. K. (1999). *Genes Dev.* **13**, 3217–3230.
Pot, I., Measday, V., Snydsman, B., Cagney, G., Fields, S., Davis, T. N., Muller, E. G. & Hieter, P. (2003). *Mol. Biol. Cell*, **14**, 460–476.
Santaguida, S. & Musacchio, A. (2009). *EMBO J.* **28**, 2511–2531.
Takeuchi, K. & Fukagawa, T. (2012). *Exp. Cell Res.* **318**, 1367–1374.
Tao, Y., Jin, C., Li, X., Qi, S., Chu, L., Niu, L., Yao, X. & Teng, M. (2012). *Nature Commun.* **3**, 782.
Tao, Y., Li, X., Liu, Y., Ruan, J., Qi, S., Niu, L. & Teng, M. (2012). *J. Biol. Chem.* **287**, 20231–20239.
Welburn, J. P. & Cheeseman, I. M. (2008). *Dev. Cell*, **15**, 645–655.
Westermann, S. & Schleiffer, A. (2013). *Trends Cell Biol.* **23**, 260–269.
Winn, M. D. *et al.* (2011). *Acta Cryst.* D**67**, 235–242.
Yuen, K. W. Y., Montpetit, B. & Hieter, P. (2005). *Curr. Opin. Cell Biol.* **17**, 576–582.